CHEMISTRY
AN ASIAN JOURNAL

DOI: 10.1002/asia.200700265

A Dicationic Organoplatinum(II) Complex Containing a Bridging 2,5-Bis-(4-ethynylphenyl)-[1,3,4]oxadiazole Ligand Behaves as a Phosphorescent Gelator for Organic Solvents

Wei Lu, Yuen-Chi Law, Jie Han, Stephen Sin-Yin Chui, Dik-Lung Ma, Nianyong Zhu, and Chi-Ming Che*[a]

Abstract: A dicationic platinum(II) terpyridyl complex, [(*t*Bu$_3$tpy)Pt(OXD)Pt(*t*Bu$_3$tpy)](PF$_6$)$_2$ (*t*Bu$_3$tpy = 4,4′,4″-tri-*tert*-butyl-2,2′:6′,2″-terpyridyl, OXD = 2,5-bis(4-ethynylphenyl)[1,3,4]oxadiazole) formed phosphorescent organogels in acetonitrile or in a mixture of acetonitrile and alcohol. The structure and properties of these emissive gels were analyzed by polarizing optical and confocal laser scanning microscopy, and by variable-temperature ^{1}H NMR, UV/Vis, and emission spectroscopy. Dry gels were studied by scanning electron microscopy, powder X-ray diffraction (PXRD), and small-angle X-ray scattering (SAXS). SEM images of the dry gel revealed a network of interwoven nanofibers (diameter 12–60 nm, length > 5 μm). Intermolecular π–π interactions between the [(*t*Bu$_3$tpy)PtC≡C] moieties could be deduced from the variable ^{1}H NMR spectra. The PXRD and SAXS data showed that the assembly of the gelator could be represented by a rectangular 2D lattice of 68 Å × 14 Å. The ability of the complex to gelate a number of organic solvents is most likely due to intermolecular π–π interactions between the [(*t*Bu$_3$tpy)PtC≡C] moieties.

Keywords: acetylides · gels · luminescence · platinum · self-assembly

Introduction

There has been growing interest in low-molecular-mass organogelators (LMMGs) owing to their potential applications in materials science, drug delivery, and for the construction of supramolecular nanostructures.[1] Organogels and hydrogels are produced by the spontaneous segregation of micro- to nanophases of gelator and solvent molecules.[2] A subtle balance between gelator–gelator and gelator–solvent interactions regulates gelator solubility and prevents crystallization.[1] Noncovalent intermolecular interactions, including π–π stacking forces, hydrogen bonding, and electrostatic and van der Waals interactions, provide the driving force for the construction of a three-dimensional supramolecular network within which the fluidity of solvent is retarded. Amphiphilic molecules that contain aromatic-linking-steroidal (ALS) moieties, multiple hydrogen-bonding motifs (such as sugar, peptide, and urea), or polycyclic aromatic hydrocarbons (PAHs) together with long alkyl chains are usually considered to be candidates for gelating organic solvents and/or water.[3] However, there is no systematic correlation between molecular structure and gelation ability, and it is still obscure how the molecular packing of gelator molecules influences the collective properties of the gel, such as light emission, mechanical properties, and thermodynamic behavior. Thus the continued development and analysis of new gelator species should enrich and deepen our general understanding of LMMGs.[1]

A number of transition-metal complexes have been investigated as low-molecular-mass gelators owing to their varied coordination geometries and rich optical properties, both of which are not accessible from organic gelators. Recently, several derivatives of bis(β-diketonate)copper(II),[4] pentacarbonyl[D-glucohex(*N*-*n*-octylamino)-1-ylidene]chromium,[5] bis(8-quinolinol)platinum(II),[6] bis(bipyridyl)copper(I),[7] triazolecobalt(II),[8] trinuclear gold(I) pyrazolate,[9]

[a] Dr. W. Lu, Dr. Y.-C. Law, Dr. J. Han, Dr. S. S.-Y. Chui, Dr. D.-L. Ma, Dr. N. Zhu, Prof. Dr. C.-M. Che
Department of Chemistry
Open Laboratory of Chemical Biology of the Institute of Molecular Technology for Drug Discovery and Synthesis, and
HKU-CAS Joint laboratory on new Materials
The University of Hong Kong
Pokfulam Road, Hong Kong SAR (China)
Fax: (+852) 2857-1586
E-mail: cmche@hku.hk

Supporting information for this article is available on the WWW under http://www.chemasianj.org or from the author.

zinc(II)–porphyrin,[10] titanocene–cholesterol,[11] terpyridyl platinum(II) acetylides,[12] and palladium(II) pincer bis(imidazolylidene)[13] have been found to gelate a number of organic solvents. Potential gelating motifs, such as amides, glucose, and cholesterol, are covalently linked to auxiliary ligands within these metal-containing gelators. Peripheral long-chain alkyl groups have also been used to isolate the "nanodomains" of the gelator molecules from each other.[14] Notably, Naota and co-workers reported that two binuclear palladium(II) complexes that bear Schiff base and dipeptide ligands, upon ultrasonic stimulation, could gelate acetone, carbon tetrachloride, and ethyl acetate.[15] Intra- and intermolecular π–π interactions for the Schiff base complex and hydrogen-bonding interactions for the dipeptide complex were suggested to be the driving forces for gelation.

Herein we describe the synthesis and properties of a low-molecular-mass phosphorescent organogelator based on a binuclear terpyridyl platinum(II) salt **1** (Scheme 1) with a

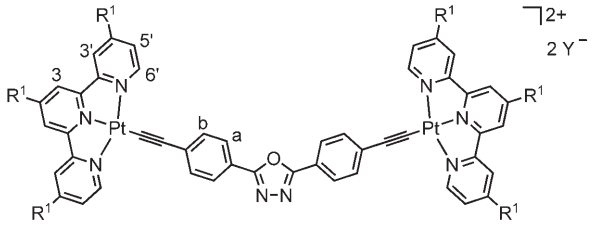

1 R^1 = *t*Bu, Y = PF_6 **2** R^1 = H, Y = OTf

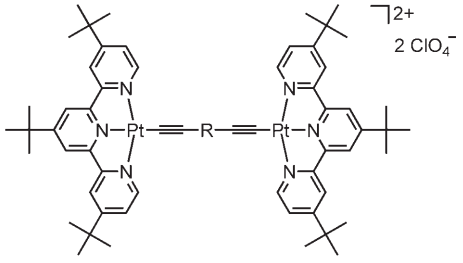

3 R = 1,3-phenylene **4** R = 4,4'-biphenylene

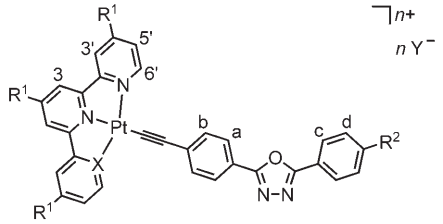

5 R^1 = *t*Bu, R^2 = $OC_{10}H_{21}$, X = N, Y = PF_6, *n* = 1

6 R^1 = *t*Bu, R^2 = CH_3, X = N, Y = ClO_4, *n* = 1

7 R^1 = *t*Bu, R^2 = $N(CH_3)_2$, X = N, Y = PF_6, *n* = 1

8 R^1 = H, R^2 = CH_3, X = C, n = 0

Scheme 1. Chemical structures of **1**–**8**.

2,5-bis(4-ethynylphenyl)-[1,3,4]oxadiazole (OXD) bridging ligand. This metal-containing gelator does not contain any long alkyl chains or recognized gelating motifs, but, to our initial surprise, acts as a gelator for acetonitrile and acetonitrile/alcohol mixtures. The binuclear complexes **2**–**4** and mononuclear complexes **5**–**8** were also synthesized for comparative studies. Platinum(II) terpyridine complexes have been widely investigated for decades owing to their intriguing biological activities and spectroscopic properties.[16] Terpyridyl/cyclometalated platinum(II) acetylides are well-known as light-emitting materials and are useful building blocks for supramolecular structures.[17] The objective of our initial investigation was to develop phosphorescent organoplatinum(II) complexes as functional molecular materials. We chose the OXD moiety to link the two terpyridyl platinum(II) chromophores because organic OXD derivatives are strongly fluorescent[18] and generally have good electron-transporting properties.[19] We reasoned that the incorporation of an angular OXD moiety into an organoplatinum(II) complex would modify its overall molecular shape as well as its emission and electronic properties. Immediately after the completion of this study, two reports[12] were published in 2007 revealing that terpyridyl platinum(II) acetylide complexes with auxiliary ligands containing multiple long alkyl chains are efficient gelators for hexane, benzene, and DMSO. The interplay between metal–metal, π–π, and hydrophobic interactions was found to be of pivotal importance for the gelation process.

Results

Synthesis and Characterization

Complexes **1**–**8** were prepared by the reaction of the appropriate platinum(II) precursors ([(*t*Bu_3tpy)PtCl]Y for **1** and **3**–**7**, [(tpy)PtCl]Y for **2**, and (C^N^N)PtCl ((HC^N^N) = 6-phenyl-2,2′-bipyridine,) for **8**) with the corresponding arylacetylide ligands in a CH_2CH_2/*i*Pr_2NH (20:1 *v*/*v*) mixture and in the presence of a catalytic amount of CuI. The crude products were purified by column chromatography on an alumina column. Complexes **1**–**8** were obtained as air-stable crystalline solids in 50–86% yields and were characterized by ^{1}H and ^{13}C NMR, and IR spectroscopy, FAB mass spectrometry, and elemental analysis. The structures of **5** and **8** were also determined by single-crystal X-ray crystallography.

Crystal Structures of 5·2MeCN and 8

The crystal-structure and -packing diagrams of the complex cations of **5**·2MeCN and **8** are shown in Figures 1 and 2, respectively. Selected bond lengths and angles are listed in the Supporting Information. All the bond lengths and angles for **5**·2MeCN and **8** are comparable to those observed in related terpyridyl/cyclometalated Pt^{II} complexes.[17,20] For **8**, the Pt–C(acetylide) distance of 1.941(8) Å is slightly shorter than that found in [(C^N^N)PtC≡CR] (R = Ar), 1.959(9)–1.98(1) Å],[17c] and the acetylenic distance of C17–C18, 1.239(9) Å, is slightly longer than those found in the cyclometalated Pt^{II} congeners (ranging from 1.184(6) to 1.22(1) Å).[17c] No close intermolecular Pt–Pt contacts with

CHEMISTRY
AN ASIAN JOURNAL

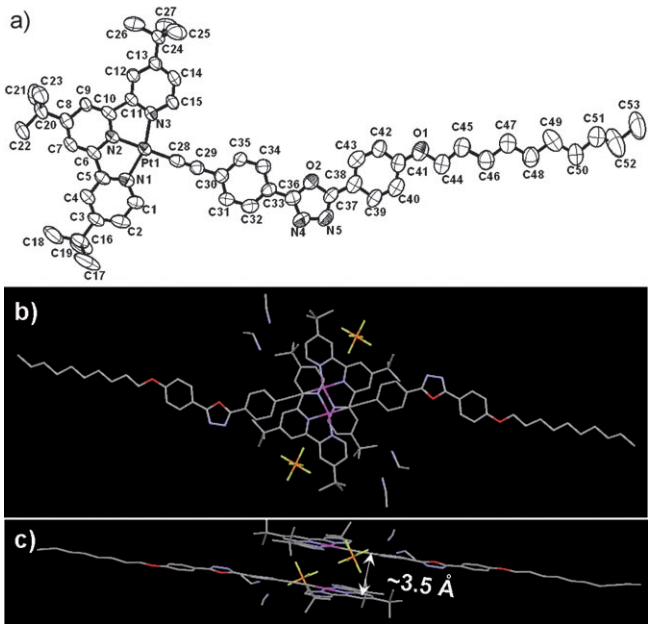

Figure 1. a) Perspective drawing of the complex cation of **5**. Hydrogen atoms are omitted for clarity. Thermal ellipsoids are shown at the 50% probability level. Crystal packing diagram of **5**·2MeCN viewed b) along *a* axis and c) perpendicular to the *ab* plane.

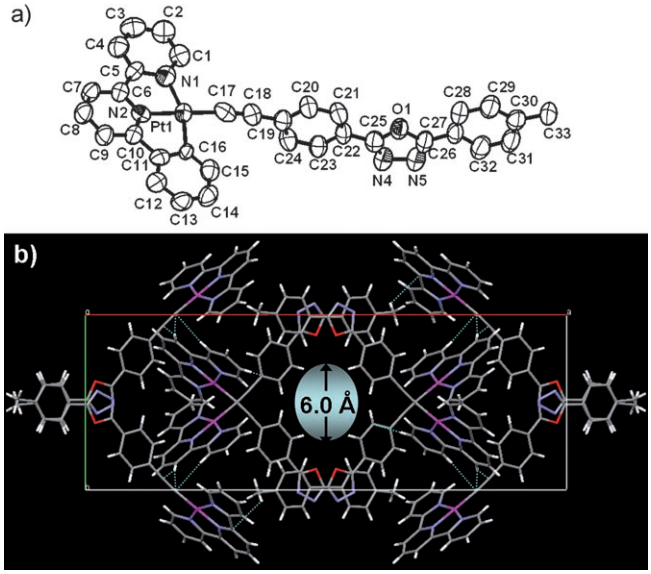

Figure 2. a) Perspective drawing of complex **8**. Hydrogen atoms are omitted for clarity. Thermal ellipsoids are shown at the 50% probability level. b) The unit cell of **8** viewed along the *c* axis shows the central channel.

d(Pt–Pt) < 4 Å were found in the crystal structures of **5**·2MeCN and **8**. For **5**·2MeCN, the 2,5-bis-phenyl[1,3,4]oxadiazole moiety is nearly coplanar with the [(tpy)Pt] plane (the dihedral angle between the Pt1–N1–N2–N3 and the C29–C30–C31–C35 planes was measured to be around 5°), and the $C_{10}H_{21}$ group adopts an extended *all-trans* configuration. The two neighboring [(tpy)Pt] planes in the crystal structure of **5**·2MeCN are stacked in head-to-tail pairs (Figure 1b) with interplanar distances of approximately 3.5 Å (Figure 1c), a value generally recognized for π–π interactions.[21] For **8**, the 2,5-bis-phenyl[1,3,4]oxadiazole moiety is almost perpendicular to the [(C^N^N)Pt] plane (the dihedral angle between the Pt1–N1–N2–N16 and the C18–C19–C20–C24 planes was measured to be around 93°). Weak intermolecular C–H···π contacts (2.80–2.90 Å, dotted blue lines in Figure 2b) between the protons of the (C^N^N) moiety and the $C_6H_4C{\equiv}C$ moiety and a channel along the *c* axis with a diameter around 6.0 Å (Figure 2b) are evident in the crystal-packing diagram of **8**.

Gelation Properties of 1

Upon warming to ≈50–60 °C followed by cooling to room temperature, **1** in acetonitrile or acetonitrile mixed with methanol, ethanol, propan-1-ol, propan-2-ol, or butan-2-ol formed a thermoreversible, transparent, orange gel. The formation of the gel could be verified easily by inverting the sample vial to see the immobilization of the solvent fluid. Figure 3 shows the orange gel formed by gelator **1**

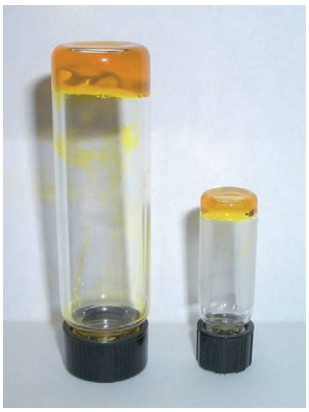

Figure 3. Image of the gel formed with **1** in CH_3CN (3.5 wt%).

(3.5 wt%) in acetonitrile. The gel-to-solution phase-transition temperature (T_{gel}) values of the gels containing gelator **1** in several different solvent systems were determined at their critical gelation concentrations (CGC), with the results listed in Table 1. The highest T_{gel} (40 °C) was found for a mixture of acetonitrile and propan-2-ol (1:1 *v*/*v*), and the lowest T_{gel} (32 °C) was found for pure acetonitrile. Upon increasing the temperature, the gel formed in acetonitrile turned into a viscous fluid more readily than that in the acetonitrile–alcohol mixture. When the free 2,5-diaryl-[1,3,4]oxadiazole ligand (1.8 wt% in acetonitrile or 4.8 wt% in dichloromethane), the binuclear complexes **2**–**4**, or the mononuclear complexes **5**–**8** were added to various organic solvents under identical conditions, there was no gel formation. Interestingly, the slow diffusion of diethyl ether into a solution of **2** in DMF (*N*,*N*-dimethylformamide) resulted in the formation of a deep brown viscous fluid.

Table 1. Gelation properties of **1**.

Solvent[a]	State[b]	T_{gel}[c] [°C]	CGC[d] [g dm^{-3}]
acetonitrile	G	32	24
methanol	P		
dichloromethane	P		
acetonitrile/methanol (1:1)	G	35	17
acetonitrile/ethanol (1:1)	G	36	15
acetonitrile/propan-2-ol (1:1)	G	40	9
acetonitrile/propan-1-ol (1:1)	G	33	9
acetonitrile/butan-2-ol (1:1)	G	35	8
acetonitrile/dichloromethane (1:1)	S		
acetonitrile/water (2.5:1)	P		
acetonitrile/methanol/ethanol (1.25:1:1)	G		11

[a] The mixture solvent is given by volume ratio. [b] G = gel; P = precipitate; S = solution at concentration of 25 g dm^{-3}. [c] Tested at CGC. [d] CGC = critical gelation concentration (the minimum concentration necessary for gelation of solvent), determined at 298 K.

Polarized Optical Microscopy of the Gel

A gel sample of **1** (7 wt% in acetonitrile) sandwiched between two glass plates was analyzed by polarizing optical microscopy (POM). The orange gel was transparent in the bright field (Figure 4a). In contrast, a textured dark field

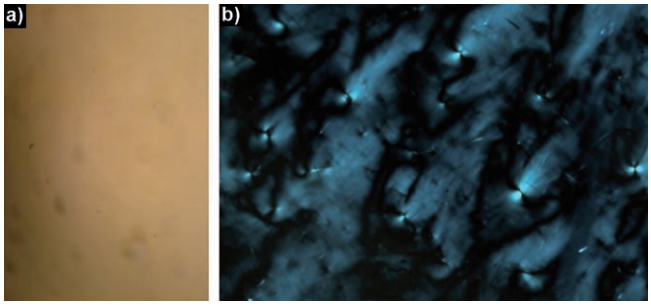

Figure 4. a) Bright-field image (100×) of the gel formed with **1** in acetonitrile (7.0 wt%). b) The same gel observed under a pair of crossed-polarizers shows Schlieren textures with two-brushed point defects (200×).

image was observed under crossed polarizers (Figure 4b). The dark area of the image was attributed to an isotropic phase that probably resulted from the acetonitrile solvent, whereas the bright area of the image is due to an anisotropic phase formed within the gel. Point defects composed of two brushes are evident in the POM images of the gel formed by **1**, revealing a topological singularity with $s = \pm 1/2$. This birefringence image observed under crossed polarizers resembles those of Schlieren textures typically observed in nematic thermotropic and lyotropic liquid crystals.[22]

Scanning Electron Microscopy of the Dry Gel

Gel samples of **1** in acetonitrile (3.5 wt%) and in mixtures of acetonitrile/propan-2-ol (1.1 wt%) or acetonitrile/propan-1-ol (1.3 wt%) were slowly evaporated to dryness, and the resultant xerogels were examined by scanning electron microscopy (SEM). The respective SEM images are shown in Figure 5a–d. A dense network of topographical fibrillar structures was observed for all samples. The morphology of the xerogel formed by gelator **1** in acetonitrile is different to

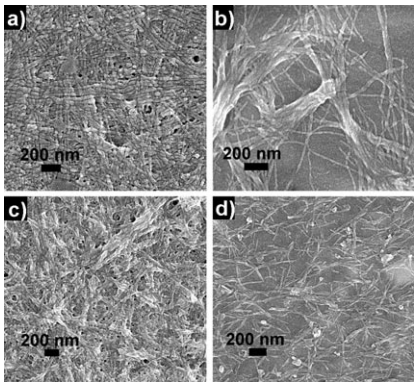

Figure 5. SEM image of a) xerogel formed with **1** in acetonitrile (3.5 wt%); b) xerogel formed with **1** in acetonitrile/propan-2-ol (1:1 *v*/*v*) (1.1 wt%); c) xerogel formed with **1** in acetonitrile/propan-1-ol (1:1 *v*/*v*) (1.3 wt%); d) viscous fluid formed by **2** in DMF/diethyl ether.

the xerogels of **1** in acetonitrile/alcohol solvent mixtures. In acetonitrile, gelator **1** was distributed into a homogeneous aggregation of fibers longer than 5 μm and with diameters of 12–20 nm (Figure 5a). When the gel was formed in acetonitrile/alcohol (propan-2-ol or propan-1-ol) mixtures, the fibers were still longer than 5 μm, but were bundled and had diameters of 30–60 nm (Figure 5b and c). Moreover, bundled nanofibers with lengths of less than 1.5 μm and diameters of around 50 nm were observed in the SEM image (Figure 5d) of the viscous fluid formed by **2** in a DMF/diethyl ether mixture.

Powder X-ray Diffraction of 1 as Xerogel

A xerogel sample of **1**, prepared by evaporating a 3.5 wt% gel of **1** in acetonitrile, was subjected to powder X-ray diffraction (PXRD) (Figure 6) and small-angle X-ray scattering

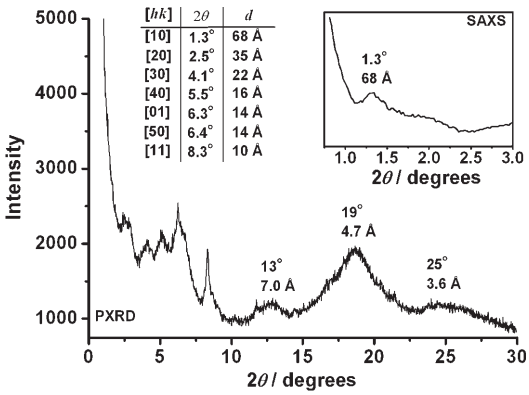

Figure 6. Powder X-ray diffraction (PXRD) and small-angle X-ray scattering (SAXS) plots (integrated intensity versus scattering angle, inset) for the xerogel of **1**. The indexed peak positions in the low-angle region of the PXRD and SAXS patterns are also listed.

(SAXS) (Figure 6, inset) measurements. The low-angle diffraction peaks ($2\theta < 10°$) in the PXRD pattern were roughly indexed based on an orthogonal 2D lattice with $a = 68$ Å and $b = 14$ Å. The long axis of this lattice was confirmed by the weak SAXS peak at 1.3° (2θ) (corresponding to a d spacing of 68 Å). There are three broad peaks at 13° ($d \approx 7.0$ Å), 19° ($d \approx 4.7$ Å), and 25° ($d \approx 3.6$ Å) in the higher-angle region of the PXRD pattern. Similar diffraction patterns were previously reported for columnar mesophases formed by disc-shaped molecules.[23–27] With reference to the report by Wegner and co-workers,[23] the $d \approx 3.6$ Å halo may be assigned to π–π interactions and the $d \approx 7.0$ Å halo, twice the π–π correlation distance, could be accredited to a doubling of the period along the c axis, pointing to a staggered arrangement of adjacent cations of **1**. Stacked π systems that contain peripheral aliphatic chains generally give rise to halos at 4.7 Å halos, which have been assigned to liquidlike packing of the aliphatic chains.[23–27]

Variable-Temperature ^{1}H NMR Spectroscopic Measurements

As gelation is highly temperature-dependent, and lower temperatures usually facilitate this process, the ^{1}H NMR spectra of a 0.21 wt% of **1** in CD_3CN (a concentration far lower than the CGC) at various temperatures were recorded and are depicted in Figure 7a. When the temperature of the CD_3CN solution was decreased from 50 to −20 °C, the resonance signal for the aromatic protons 6′-H, 3-H, 3′-H, and 5-H on the terpyridyl ligand shifted upfield from $\delta = 9.14$, 8.36, 8.33, and 7.79 ppm to $\delta = 8.94$, 8.15, 8.17, and 7.62 ppm, respectively. However, the signal for Ha on the OXD moiety shifted downfield from $\delta = 8.12$ ppm to $\delta = 8.19$ ppm and the signal corresponding to H_b remained constant. The ^{1}H NMR spectra of a more-concentrated solution of **1** (1.5 wt%) in CD_3CN were also recorded at various temperatures. The integration ratio of the aromatic protons relative to that of the protons of the non-deuterated solvent residue decreased at lower temperatures. A dramatic broadening of all the signals was observed at temperatures ≤0 °C, which is consistent with virtually complete gel formation under these conditions.

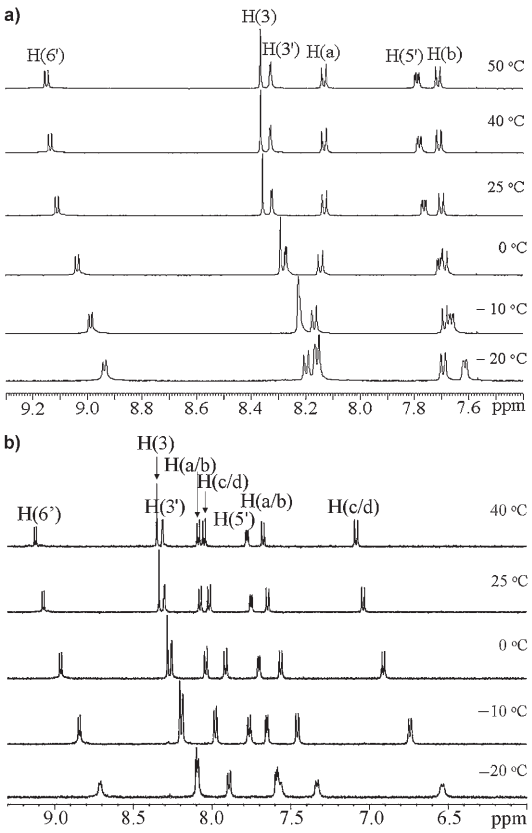

Figure 7. Variable-temperature ^{1}H NMR spectra of a) **1** and b) **5** in CD_3CN (500 MHz, 1.0×10^{-3} mol dm^{-3}). See Scheme 1 for labeling of the hydrogen atoms.

The mononuclear complex **5**, which contains the [(tBu$_3$tpy)Pt] moiety and a OXD ligand substituted with a long alkyl chain, did not gelate acetonitrile under any of the conditions tested. Its ^{1}H NMR spectra at various temperatures were also acquired (Figure 7b). The protons on the OXD moiety were found to behave quite differently to those in gelator **1**. When the temperature of a solution of **5** in CD_3CN was decreased from 40 to −20 °C, the resonance signal for the aromatic protons H_a/H_b and H_c/H_d on the OXD moiety shifted upfield from $\delta = 8.08$/7.68 ppm and $\delta =$ 8.05/7.08 ppm to $\delta = 7.88$/7.34 ppm and $\delta = 7.56$/6.53 ppm, respectively; and the aromatic protons 6′-H, 3-H, 3′-H, and 5-H on the terpyridyl ligand shifted upfield from $\delta = 9.12$, 8.36, 8.31, and 7.77 ppm to $\delta = 8.71$, 8.10, 8.08, and 7.58 ppm, respectively.

Absorption and Steady-State Emission Spectroscopy

Absorption and steady-state emission spectra were recorded for solutions of **1**–**8** in dichloromethane; detailed spectroscopic data of **1**–**8** are listed in Table S1 (Supporting Information). At $\lambda < 400$ nm, **1**–**8** display vibronically structured absorption bands with extinction coefficients $> 5.0 \times 10^4$ dm^3 mol^{-1} cm^{-1}, which are within the range of ε values previously determined for the $^1(\pi$–$\pi^*)$ transitions of OXD and terpyridine or (C^N^N) ligands.[17] The binuclear complexes **1** and **2** and the mononuclear complexes **5**–**7** have similar absorption energies but different extinction coefficients at 400–600 nm. The broad, low-energy bands with λ_{max} in the 412—475-nm region and $\varepsilon < 1.6 \times 10^4$ dm^3 mol^{-1} cm^{-1} are comparable with the low-energy ^{1}MLCT transitions of the related complexes [(tBu$_3$tpy)PtCH$_2$C(O)CH$_3$]ClO$_4$,[20] [(tpy)PtC≡CC$_6$H$_4$R]PF$_6$,[17a] and [(C^N^N)PtC≡CC$_6$H$_4$R].[17c] Consequently, these are assigned as transitions with an admixture of ^{1}LLCT[π(OXD)→π*(terpy or C^N^N)] and ^{1}MLCT[$d\pi$(Pt)→π*(terpy or C^N^N)] character. When the substituent R^2 on the OXD ligand of the mononuclear Pt^{II} complexes was changed from methyl in **6** to OC$_{10}$H$_{21}$ in **5** and to N(CH$_3$)$_2$ in **7**, a slight red shift of the peak maximum from 438 nm for **6** to 441 nm for **5** and to 464 nm for **7** was observed. The low-energy band in the UV/Vis absorption spectrum of **5** in CH_2Cl_2 is comparable to

that of **1**, except that the ε value of the latter ($\lambda_{max}=463$ nm, $\varepsilon=1.5\times10^4$ dm^{3}mol^{-1}cm^{-1}) is about twice that of the former ($\lambda_{max}=460$ nm, $\varepsilon=7.0\times10^3$ dm^{3}mol^{-1}cm^{-1}).

Complexes **1**–**8** show emissions with peak maxima at 574–609 nm, with lifetimes in the microsecond regime in degassed solutions in CH_2Cl_2 at 298 K. Complexes **1**, **5**, and **6** display relatively higher emission quantum yields of 0.23–0.31, whereas **8** has a low quantum yield of 0.09. Complexes **4** and **7** are weakly emissive (quantum yields <0.01) in CH_2Cl_2 at 298 K. The emission λ_{max} of **1** is solvent-sensitive and undergoes a blue shift from 591 nm in chloroform to 565 nm in acetonitrile at 298 K. No detectable emission from methanol or DMSO solutions of **1** was recorded. When the bridging acetylide ligand between the two [(*t*Bu$_3$tpy)Pt] moieties was changed from [1,3,4]oxadiazole (for **1**) to 4,4′-diphenylene (for **4**), the emission underwent a red shift (emission $\lambda_{max}=574$ nm (**1**) and 609 nm (**4**)). Although the cyclometalated mononuclear complex **8** and the terpyridyl congener **6** contain the same ancillary acetylide ligand, **8** shows a slightly blue-shifted emission maximum ($\lambda_{max}=568$ nm) relative to that of **6** (λ_{max} 574 nm).

Complexes **1**–**8** are emissive in the solid state at both 77 and 298 K. In general, the low-temperature solid-state emission profiles of **1**–**8** are structured with $\lambda_{max}=596$–814 nm. The difference in the substituents on the terpyridyl ligand affects the solid-state emission energy of **1** and **2**. Complex **2**, with unsubstituted terpyridyl ligands, has the more-red-shifted emission $\lambda_{max}=798$ nm at 298 K and 814 nm at 77 K relative to that of **1** ($\lambda_{max}=601$ nm at 298 K and 575 nm at 77 K), which contains bulky *tert*-butyl-substituted terpyridyl ligands. The low-temperature emission spectra of **1**–**8** in *n*-butyronitrile (*n*PrCN) solutions at 77 K were examined. Under these conditions, the emission λ_{max} of **7** (532 nm) undergoes a slight red shift relative to those of the mononuclear counterparts **5** (526 nm) and **6** (525 nm). Complex **4** shows an emission at $\lambda_{max}=545$ nm which shows a red shift relative to that obtained for glassy solutions of **1** ($\lambda_{max}=$ 526 nm) in *n*PrCN at 77 K. Slightly red-shifted emissions were also observed for *n*PrCN glassy solutions of **6** and **8** at 77 K with $\lambda_{max}=525$ nm for **6** and $\lambda_{max}=534$ nm for **8**.

We studied the absorption and emission spectra of the gel state of **1** (3.5 wt% in acetonitrile) and solutions of **1** in various organic solvents (methanol, acetonitrile, acetone, and chloroform), with spectra shown in Figure 8a and b, respectively. The salient features of the solution absorption spectra are that the allowed transitions in the 400—500-nm range are solvent-sensitive. The absorption edge of the lowest-energy transition band progressively underwent a red shift when the solvent was varied from methanol to acetonitrile, acetone, chloroform, and dichloromethane. The gel state (3.5 wt% in acetonitrile) of **1** exhibits a broad absorption with $\lambda_{max}=461$ nm, which shows a red shift relative to the analogous absorption band ($\lambda_{max}=421$ nm) in the solution state (0.02 wt% in acetonitrile), but is comparable to that recorded for a solution of **1** in dichloromethane ($\lambda_{max}=$ 463 nm). The emission spectrum of a gel sample of **1** (3.5 wt%) in acetonitrile was recorded and is shown in Figure 8b. The emission from the gel state of **1** showed a peak maximum at 563 nm together with a broad shoulder at ≈600 nm. The emission energies of the peak maximum and the shoulder are comparable to those recorded for the acetonitrile solution (peak maximum 565 nm, lifetime 1.2 μs, quantum yield 0.06) and the powder solid sample of **1** (peak maximum 601 nm, lifetime 1.0 μs), respectively. The emissive nature of **1** in the gel state (3.5 wt% in acetonitrile) was also confirmed by the observed red-light-emitting nanofibers (Figure 8b, inset) under confocal laser scanning microscopy (CLSM).

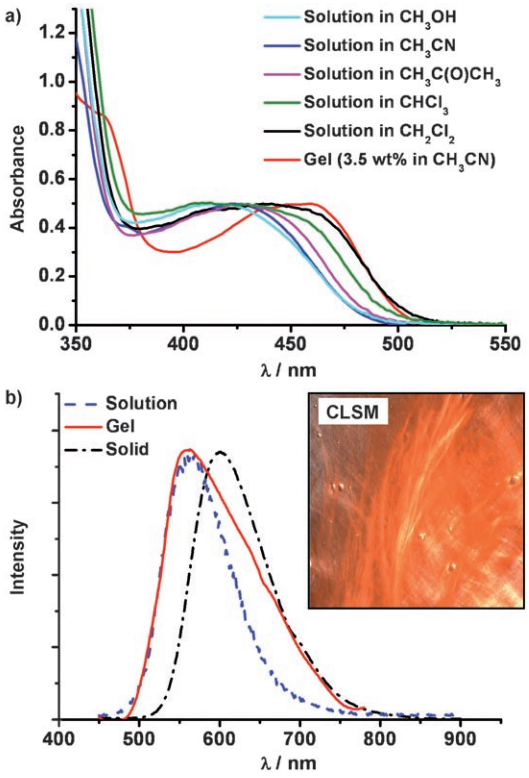

Figure 8. a) UV/Vis absorption spectra (normalized at the lowest allowed transitions) of **1** in various solutions (concentrations $\approx1\times10^{-5}$ mol dm^{-3}) and in the gel state. b) Normalized emission spectra of **1** in various states. All measurements were carried out under ambient conditions. Solution: 0.02 wt% in acetonitrile; $\lambda_{ex}=430$ nm. Gel: 3.4 wt% in acetonitrile, sandwiched between two glass plates; $\lambda_{ex}=400$ nm. Powder solid: $\lambda_{ex}=$ 430 nm. Inset: CLSM of the gel formed with **1** (3.5 wt% in acetonitrile; irradiated at 488 nm; image shows an area of 0.17×0.17 μm^2).

Discussion

Nature of the Gel Formed with 1

The gels formed by **1** in acetonitrile are semisolids or viscous fluids with anisotropic domains (see the POM Schlieren textures revealed for the gel at 7 wt% concentration), composed of microscopic networks constructed by interwoven nanofibers. A proposed structural model for the gel is depicted in Figure 9b and c, based on the estimated molecular dimensions of **1** (33 Å × 14 Å, Figure 9a) combined with

CHEMISTRY
AN ASIAN JOURNAL

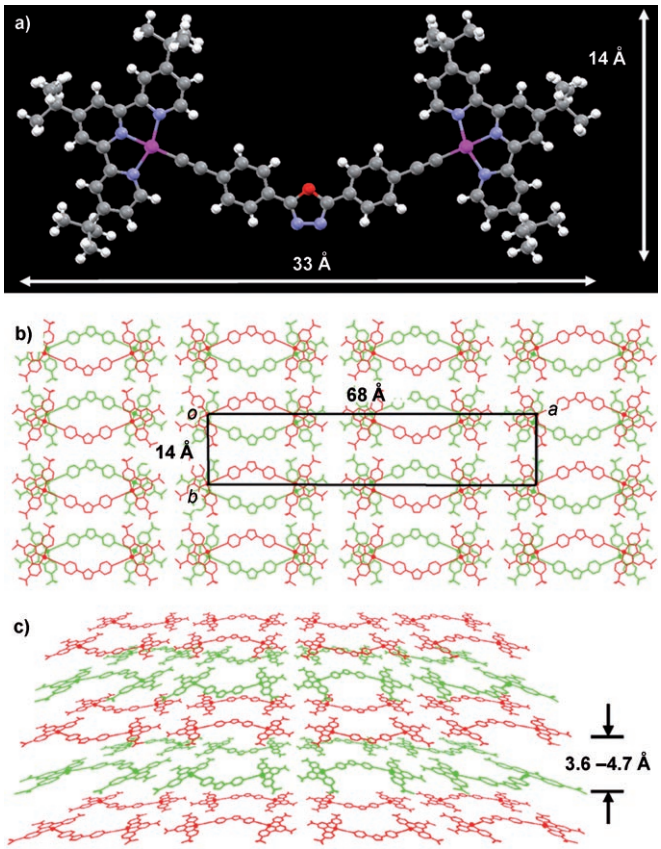

Figure 9. a) Estimated molecular size of **1**. b) Proposed layered molecular networks of **1** in the dry gel viewed along the [001] direction. c) Perspective view of the proposed layered molecular networks of **1** in the dry gel. The alternating layers are drawn in different colors and the counter ions are not shown.

the data from the PXRD and SAXS studies (Figure 6). The molecular arrangement of **1** in the dry gel could be described by a disordered structural model containing dynamically variable interlayer separations, which is evidenced by the broad peaks at $d=4.7$ Å and $d\approx3.6$ Å in the PXRD. Notably, these interlayer distances are consistent with those found for the one-dimensionally aligned bis(8-quinolinol) platinum(II) (≈4.5 Å),[6a] tetrathiafulvalene (TTF) (4.4 Å),[25] helicene,[26] hexabenzocoronene,[27] and poly(3-alkylthiophene)[28] moieties in organogels and organic nanofibers characterized previously. Because no long aliphatic chains are present in **1**, we suggest that the peak at 4.7 Å, previously assigned to aliphatic chains packed in a liquidlike arrangement in discotic liquid crystals,[24] is derived from the packing of the *tert*-butyl groups of tBu$_3$tpy moieties and/or the ClO_4^- counterions that are presumed to occupy the voids generated by the cations of **1**. The fact that all the high-angle diffractions shown in Figure 6 are broad indicates that the cations in the dry gel of **1** may fluctuate from exact parallelism. The proposed anti- (or head-to-tail) orientation of adjacent cations of **1** in the gel state is consistent with the crystal structure of **5** and the finding that all other [(tpy)Pt^{II}] complexes reported in the literature adopt a similar packing arrangement in their crystal structures. Notably, this packing model is also consistent with the halo observed at $d=7.0$ Å in the PXRD, which is a doubling of the $d=3.6$ Å diffraction peak, and with the finding from the variable-temperature ^{1}H NMR measurements, which show that the terpyridyl planes of the molecules of **1** are involved in intermolecular interactions in solution at low temperatures, but the OXD moieties are not.

Driving Force for Gelation

We identified intermolecular π–π interactions between the [(tBu$_3$tpy)PtC≡C] moieties as one of the driving forces for gelation with **1**, by correlating the structural data with the findings from variable-temperature ^{1}H NMR, absorption, and emission experiments.

The network of fibers in the gel structure could be formed by the interplay between noncovalent interactions such as hydrogen-bonding, electrostatic, π–π, metal–metal, and van der Waals interactions. Hydrogen-bonding interactions dominate in low-molecular-mass organogelators that contain amide and/or urea groups.[1] Gelator **1** does not contain any conventional hydrogen-bonding moieties, hence hydrogen-bonding interactions were not considered to be a significant factor behind gel formation with **1**. Van der Waals or London dispersion forces are ubiquitous, and these were proposed to be the stimuli for gelation with alkane gelators that contain neither hydrogen-bonding nor π–π interacting motifs.[29] Any complex cations should experience electrostatic interactions when they are placed in a gel. As gelator **1** is a dicationic platinum(II) complex, electrostatic interactions between the platinum(II) cations and the PF_6^- anions must exist extensively in the gel state of **1**. Therefore, there are two noncovalent interactions, Pt^{II}···Pt^{II} and π–π interactions, that could be specifically considered to provide the driving force for the self-assembly of **1** in the gel phase.

A number of spectroscopic and crystallographic results support the occurrence of Pt^{II}···Pt^{II} and π–π interactions in platinum(II) complexes.[16,17,20] Notably, the ^{3}MMLCT emission from the red form of the [(tpy)PtCl](ClO_4) salt, which contains relatively short Pt^{II}···Pt^{II} contacts of 3.27 Å in the solid state, occurs at 725 nm. In contrast, the excimeric intraligand emission from the orange form of [(tpy)PtCl](PF_6) occurs at 640 nm.[16e] Spectroscopic "signatures" for Pt^{II}···Pt^{II} interactions in cyclometalated and terpyridyl Pt^{II} complexes include a distinct absorption band at >500 nm and/or a low-energy emission at >650 nm. If Pt^{II}···Pt^{II} interactions exist between the [(tBu$_3$tpy)PtC≡C] moieties in the gel state of **1**, there should be significant red shifts in both the absorption and emission energies from those of **1** in solutions. Thus the Pt^{II}···Pt^{II} interactions are not evident, judging from the emission profile ($\lambda_{max}=563$ nm) of **1** in the gel state. This is consistent with the bulk of the tris(*tert*-butyl) groups, which prevents the close contact of neighboring [(tBu$_3$tpy)PtC≡C]$^+$ cations. Indeed, we found no evidence for ^{3}MMLCT emission from gelator **1** in solution or in the crystalline solid state.

With reference to previous works,[16,17,20] the "tailing-off" of the red-shifted absorption in the 400—500-nm range for gelator **1** (3.5 wt% in acetonitrile) could be explained by microenvironmental effects (such as solvent polarity and medium rigidity) and/or intermolecular aggregations. There are two major intermolecular interactions, namely ligand–ligand (π–π) and metal–metal ($Pt^{II}\cdots Pt^{II}$) interactions, that may be responsible for the aggregation of [(tpy)Pt^{II}] chromophores in the solid state. However, the red shift in low-energy absorption maximum from 421 nm for a dilute solution in acetonitrile to 461 nm for a gel of **1** (together with the emission data, as discussed above) is not significant enough to support an unambiguous assignment of a [5d-(Pt···Pt)→π*(ligand)] metal–metal-to-ligand charge-transfer (MMLCT) transition.

From the variable-temperature ^{1}H NMR spectra of **1** and **5**, it is evident that the [(*t*Bu$_3$tpy)PtC≡C] moieties within molecules of **1** or **5** progressively associate with each other through intermolecular π–π interactions with decreasing temperature. Stacked π–π structures are commonly found in the crystal structures of [(tpy)Pt^{II}] complexes.[16,17,20] Intermolecular π–π interactions can be identified in the X-ray crystal structure of **5**, in which two planar cations of **5** stack into a dimeric structure with the [(*t*Bu$_3$tpy)PtC≡C] moieties oriented in a head-to-tail fashion with an interplanar distance of ≈3.5 Å, which is a typical value for π–π interactions in square-planar platinum(II) complexes.[21b]

Structural considerations for organoplatinum(II) gelators

A number of platinum(II) complexes, **2**—**8**, were studied in order to probe structural requirements for gelators. The bridging OXD ligand, the cationic nature, and the tris(*tert*-butyl) group, may synergistically and subtly balance the molecular packing, solubility, and gelator–solvent interactions in gels formed by **1**. The angular OXD linker confers a bent shape on molecules of **1** and allows them to be packed into a compact superstructure in which the neighboring [(*t*Bu$_3$tpy)PtC≡C] moieties are associated and the OXD moieties are oriented opposite to one another (Figure 9). The bulky tris(*tert*-butyl) groups play a crucial role in balancing the solubility and gel-formation properties of **1** in organic solvents. Complex **2** has no substituents on the terpyridyl ligands and is poorly soluble in DMF and DMSO. However, fibrillar nanostructures were found in the SEM image of the DMF/Et_2O dispersion of this complex. Long aliphatic chains do not appear to be necessary for [(*t*Bu$_3$tpy)PtC≡C] complexes that contain an angular OXD ligand to act as gelators for organic solvents.

Conclusion

A dicationic platinum(II) complex that contains no conventional gel-forming motifs was found to behave as a phosphorescent organogelator. A number of structurally related Pt^{II} complexes were prepared to probe the structural and electronic factors that affect the gel-formation properties of **1**. We envisage that transition-metal complexes with related structures may provide exciting new opportunities for the future molecular design of low-molecular-mass gelators. Our findings not only add to our general understanding of organometallic supramolecular chemistry, but also suggest additional uses and applications for organoplatinum(II) complexes, such as in sol-gel polymerization or in the fabrication of soft materials for sensory applications.

Experimental Section

General Procedures

All starting materials were purchased from commercial sources and used as received unless stated otherwise. The solvents used for synthesis were of analytical grade. [(*t*Bu$_3$tpy)PtCl]ClO_4, [(*t*Bu$_3$tpy)PtCl]PF_6,[20] [(tpy)PtCl]OTf,[17a] [(C^N^N)PtCl],[17c] and 2,5-diaryl-[1,3,4]oxadiazole derivatives[18,19] were synthesized by literature methods. (*Caution*! Perchlorate salts are potentially explosive and should be handled with care and in small amounts.) For the preparation of the gel samples, the solvents were of both analytical and HPLC grade. Complex **1** was placed in a screw-cap vial, and the solvent (or solvent mixture) was added by autopipette exposed to air. Solutions of **1** were obtained by heating these mixtures in a water bath (50–60 °C). Afterwards, the samples were cooled to room temperature for the determination of the T_{gel} values. Samples for SEM were prepared by immersing a copper grid into the gel and allowing it to dry in air overnight. All the samples for SEM were sputtered with gold thin film (20 second, <2 nm thickness). For the determination of T_{gel}, the gel of **1** was prepared in a screw-cap vial. The vial was wrapped with water-proof film, and then placed inverted into a water bath. As soon as the gel started to float down the surface of container, the corresponding temperature was denoted as T_{gel}. A small portion of gel **1** (7 wt% in acetonitrile) was taken out and sanwiched between two glass plates for examination under the polarizing optical microscope.

Physical Measurements and Instrumentation

^{1}H NMR (500 MHz) and ^{13}C NMR (126 MHz) spectra were recorded on a DPX 500 Brucker FT-NMR spectrometer; the chemical shifts (in ppm) are reported relative to nondeuterated solvent residual as reference. Positive-ion-mode FAB mass spectra and EI mass spectra were recorded on a Finnigan Mat 95 mass spectrometer. Positive-ion-mode ESI mass spectra were recorded on a Finnigan LCQ mass spectrometer. Elemental analyses of the new complexes were performed at the Institute of Chemistry at the Chinese Academy of Sciences, Beijing. UV/Vis absorption spectra were recorded on a Hewlett–Packard 8452A diode array spectrophotometer or on a Perkin-Lambda 19 UV/Vis spectrophotometer. The SEM images were taken on a LEO 1530 scanning electron microscope operating at 5.0 kV. The polarizing optical images were taken on a Olympus BX51 microscope.

Emission and Lifetime Measurements

Steady-state excitation and emission spectra were obtained on a SPEX Fluorolog-3 spectrophotometer. All solutions for photophysical studies were degassed by using a high-vacuum line in a two-compartment cell consisting of a 10-mL pyrex bulb and a 1-cm-pathlength quartz cuvette sealed from the atmosphere by a Bibby Rotaflo HP6 Telfon stopper. The solutions used for emission measurements were subjected to no less than four freeze-pump-thaw cycles. For low-temperature (77 K) emission spectra, the *n*PrCN glassy solutions and solid-state samples were loaded in 5-mm-diameter quartz tubes that were immersed into a liquid-nitrogen Dewar flask equipped with quartz windows. The emission spectra were corrected for monochromator and photomultiplier efficiency and for xenon-lamp stability. Emission lifetime measurements were performed with a Quanta Ray DCR-3 pulsed Nd:YAG laser system (pulse output 355 nm, 8 ns). Errors for λ values (+1 nm), τ (+10%), and ϕ (+10%)

are estimated. Luminescence quantum yields were measured relative to a degassed acetonitrile solution of $[Ru(bpy)_3](PF_6)_2$ as a standard reference ($\Phi_r = 0.062$).

Powder X-ray Diffraction and Small-Angle X-ray Scattering Measurements

Overnight powder X-ray diffraction data acquisition was conducted at a scan speed of 10 seconds per step (step size = 0.02°) on a Bruker D8 X-ray powder diffractometer with $Cu_{K\alpha}$ radiation ($\lambda = 1.5418$ Å). Small-angle X-ray scattering data was acquired on a Bruker NANOSTAR U system with a ceramic sealed X-ray tube ($Cu_{K\alpha}$ $\lambda = 1.5418$ Å rated at 1.2 kW). The divergent X-ray was prealigned with two multilayer Göbel mirrors oriented in the horizontal and vertical directions. The incident X-ray beam (0.6×0.6 mm^2) was collimated by using three pin-holes, and the solid sample was mounted on adhesive tape (Scotch 3M). Positioning of the sample holder was driven by a computer-controlled XY-gonoimeter. Data collection was carried out in a sealed sample chamber under a dynamic vacuum of 2×10^{-3} mbar. The scattering signal was measured by a two-dimensional detector (HI-STAR). The sample-to-detector distance (1050 mm) was precalibrated with the d value of the first-order diffraction ring ($2\theta = 1.514°$, $d = 58.354$ Å) of a standard silver behenate ($C_{21}H_{43}CO_2Ag$). The raw scattering data was corrected for the intensity variations due to spatial aberrations and uniformity of the 2D detector. The peak maxima of the scattered signal were automatically determined by radial integration along the χ direction ($2\theta = 1.0$–$3.0°$, χ angle range = 0–355°) of the scattering pattern. The results were plotted as normalized intensity versus scattering angle (I vs. 2θ) by using the SAXS NT (Bruker AXS) program.

Syntheses and Characterization

1: The bridging OXD ligand (0.10 mmol) was added to a solution of $[(t\text{Bu}_3\text{tpy})\text{PtCl}]\text{PF}_6$[14] (0.146 g, 0.20 mmol), CuI (0.01 g, 0.05 mmol), and diisopropylamine (1 mL) in dichloromethane (20 mL). The resultant solution mixture was stirred at room temperature under a nitrogen atmosphere for 12 h. The mixture was evaporated to dryness, dissolved in dichloromethane, and loaded onto an alumina (neutral) column. The product (yellow band, $R_f = 0.38$) was eluted with CH_2Cl_2/MeCN (4:1 v/v) and upon evaporation to give $[(t\text{Bu}_3\text{tpy})\text{Pt(oxd)Pt}(t\text{Bu}_3\text{tpy})](\text{PF}_6)_2$ (**1**) as an orange solid (100 mg, 60 %). ^{1}H NMR (500 MHz, CD_3CN, 25 °C, TMS): $\delta = 1.47$ (s, 18H; *t*Bu), 1.54 (s, 36H; *t*Bu), 7.69 (d, 4H, $^3J_{HH} = 8.4$ Hz; a/b-H), 7.76 (dd, 4H, $^3J_{HH} = 6.0$ Hz, $^4J_{HH} = 2.0$ Hz; 5-H), 8.13 (d, 4H, $^3J_{HH} = 8.4$ Hz; a/b-H), 8.32 (d, 4H, $^4J_{HH} = 1.7$ Hz; 3-H), 8.35 (s, 4H; 3′-H), 9.11 ppm (d, 4H, $^3J_{HH} = 6.0$ Hz; 6-H); $^{13}C\{^1H\}$ NMR (126 MHz, CD_3CN, 25 °C, TMS): $\delta = 30.3$, 30.6, 37.1, 38.1, 104.3 (PtC≡*C*), 104.5 (Pt*C*≡C), 122.3, 122.6, 124.3, 126.9, 127.6, 131.6, 133.5 (aryl C), 154.9, 155.1, 159.7, 165.3, 168.0, 168.7 ppm; IR (nujol): $\tilde{\nu} = 2113$ cm^{-1} (m, C≡C); MS (FAB, +ve, NBA matrix): m/z: 1561 $[\mathbf{1}-\text{ClO}_4]^+$, 730 $[\mathbf{1}-2\,\text{ClO}_4]^{2+}$; elemental analysis: calcd (%) for $C_{72}H_{78}N_8OClP_2F_{12}Pt_2$: C 49.37, H 4.49, N 6.40; found: C 49.81, H 4.21, N 6.70.

2: The preparation was similar to that for **1** except that [(tpy)PtCl]OTf was used instead of $[(t\text{Bu}_3\text{tpy})\text{PtCl}]\text{ClO}_4$. The mixture was stirred for 12 h, evaporated to dryness, washed with acetonitrile, and dried under vacuum to give a brown shiny solid $[(\text{tpy})\text{Pt(oxd)Pt(tpy)}](\text{OTf})_2$ (**2**) (80 mg, 80 %). ^{1}H NMR (500 MHz, [D$_6$]DMSO, 25 °C, TMS): $\delta = 7.76$ (d, 4H, $^3J_{HH} = 8.4$ Hz; a/b-H), 7.96 (t, 4H, $^3J_{HH} = 6.7$ Hz; 5-H), 8.13 (d, 4H, $^3J_{HH} = 8.3$ Hz; a/b-H), 8.53 (t, 4H, $^3J_{HH} = 7.8$ Hz; 4-H), 8.59–8.62 (m, 2H, $^3J_{HH} = 8.4$ Hz; 4′-H), 8.67 (t, 8H, $^3J_{HH} = 8.4$ Hz; 3-H), 9.22 ppm (d, 4H, $^3J_{HH} = 4.6$ Hz; H$_6$); $^{13}C\{^1H\}$ NMR (126 MHz, [D$_6$]DMSO, 25 °C, TMS): $\delta = 103.4$ (PtC≡*C*), 104.1 (Pt*C*≡C), 120.9, 124.2, 125.9, 126.6, 129.8, 130.3, 132.6, 142.3, 153.9, 154.4, 158.6, 163.9, 173.3 ppm; IR (nujol): $\tilde{\nu} = 2118$ cm^{-1} (m, C≡C); MS (FAB, +ve NBA matrix): m/z: 1125 $[\mathbf{2}-2\,\text{OTf}-\text{H}]^+$; elemental analysis: calcd (%) for $C_{50}H_{30}N_8O_7Pt_2F_6S_2$: C 42.20, H 2.12, N 7.87; found: C 42.03, H 2.52, N 7.70.

3: The preparation was similar to that for **1** except that 1,3-diethynylbenzene was used instead of the OXD ligand. The mixture was stirred for 12 h, evaporated to dryness, dissolved in dichloromethane, and loaded onto an alumina (neutral) column. The orange band was eluted with CH_2Cl_2, and evaporation of the solvent gave $[(t\text{Bu}_3\text{tpy})\text{PtC}\equiv\text{C}(1,3\text{-phenylene})\text{C}\equiv\text{CPt}(t\text{Bu}_3\text{tpy})](\text{ClO}_4)_2$ (**3**) as an orange solid (103 mg, 68 %). ^{1}H NMR (500 MHz, CD_3CN, 25 °C, TMS): $\delta = 1.40$ (s, 36H; *t*Bu), 1.49 (s, 18H; *t*Bu), 7.26–7.30 (m, 3H; C_6H_4), 7.61 (dd, 4H, $^3J_{HH} = 2.0$; 6.0 Hz; 5-H), 7.84, (s, 1H; C_6H_4), 8.20 (d, 4H, $^3J_{HH} = 2.0$ Hz; 3-H), 8.25 (s, 4H; 3′-H), 9.04 ppm (d, 4H, $^3J_{HH} = 6.0$ Hz; 6-H); $^{13}C\{^1H\}$ NMR (126 MHz, CD_3CN, 25 °C, TMS): $\delta = 30.3$, 30.7, 37.1, 38.1, 100.4 (PtC≡*C*), 104.7 (Pt*C*≡C), 122.2, 124.1, 126.8, 128.2, 129.4, 130.8, 136.5, 155.0, 155.1, 159.6, 167.7, 168.5 ppm; IR (nujol): $\tilde{\nu} = 2113$ cm^{-1} (w, C≡C); MS (ESI): m/z; 1417 $[\mathbf{3}-\text{ClO}_4]^+$, 659 $[1/2(\mathbf{3}-2\,\text{ClO}_4)]^+$; elemental analysis: calcd (%) for $C_{69}H_{88}N_6O_8Cl_2Pt_2\cdot H_2O$: C 51.52, H 5.64, N 5.22; found: C 51.21, H 5.91, N 5.10.

4: The preparation was similar to that for **1** except that 4,4′-diethynylbiphenyl was used instead of the OXD ligand. The mixture was stirred for 12 h, evaporated to dryness, dissolved in dichloromethane, and loaded onto an alumina (neutral) column. The orange band was eluted with CH_2Cl_2, and evaporation of the solvent gave $[(t\text{Bu}_3\text{tpy})\text{PtC}\equiv\text{C}(4,4'\text{-biphenylene})\text{C}\equiv\text{CPt}(t\text{Bu}_3\text{tpy})](\text{ClO}_4)_2$ (**4**) as an orange solid (95 mg, 60 %). ^{1}H NMR (500 MHz, [D$_6$]DMSO, 25 °C, TMS): $\delta = 1.45$ (s, 36H; *t*Bu), 1.53 (s, 18H; *t*Bu), 7.58 (d, 4H, $^3J_{HH} = 8.4$ Hz; C_6H_4), 7.70 (d, 4H, $^3J_{HH} = 8.3$ Hz; C_6H_4), 7.92 (dd, 4H, $^3J_{HH} = 6.1$ Hz, $^4J_{HH} = 1.9$ Hz; 5-H), 8.71 (d, 4H, $^4J_{HH} = 1.7$ Hz; 3-H), 8.72 (s, 4H; 3′-H), 9.06 ppm (d, 2H, $^3J_{HH} = 6.0$ Hz; 6-H); $^{13}C\{^1H\}$ NMR (126 MHz, [D$_6$]DMSO, 25 °C, TMS): $\delta = 29.8$, 30.3, 36.2, 37.2, 101.0 (PtC≡*C*), 103.3 (Pt*C*≡C), 121.5, 123.6, 125.9, 126.0, 126.2, 132.2, 137.3, 153.7, 158.5, 166.4, 167.0 ppm; IR (nujol): $\tilde{\nu} = 2116$ cm^{-1} (w, C≡C); MS (FAB, +ve NBA matrix): m/z: 1494 $[\mathbf{4}-\text{ClO}_4]^+$, 1393 $[\mathbf{4}-2\,\text{ClO}_4-\text{H}]^+$; elemental analysis: calcd (%) for $C_{75}H_{92}N_6O_8Cl_2Pt_2\cdot H_2O$: C 53.47, H 5.62, N 4.99; found: C 53.08, H 5.57, N 4.98.

5: 2-(4-Decyloxyphenyl)-5-(4-ethynylphenyl)-[1,3,4]oxadiazole (0.1 mmol) was added to a yellow solution of $[(t\text{Bu}_3\text{tpy})\text{PtCl}]\text{PF}_6$ (76 mg, 0.10 mmol), CuI (0.01 g, 0.05 mmol), and diisopropylamine (1 mL) in dichloromethane (10 mL). The resultant solution mixture was stirred at room temperature under inert atmosphere for 12 h. The mixture was evaporated to dryness, dissolved in dichloromethane, and loaded onto an alumina (neutral) column. The orange band was eluted with CH_2Cl_2, and a yellow band ($R_f = 0.14$) was isolated. Yellow needles of $[(t\text{Bu}_3\text{tpy})\text{PtC}\equiv\text{CC}_6\text{H}_4\text{-C}_2\text{N}_2\text{O-C}_6\text{H}_4\text{-OC}_{10}\text{H}_{21}](\text{PF}_6)$ (**5**) were obtained by vapor diffusion of diethyl ether into a solution in acetonitrile (40 mg, 55 %). ^{1}H NMR (500 MHz, CD_3CN, 25 °C, TMS): $\delta = 0.88$ (t, 3H, $^3J_{HH} = 7.0$ Hz; $OCH_2CH_2C_7H_{14}CH_3$), 1.26–1.37 (m, 14H; $OCH_2CH_2C_7H_{14}CH_3$), 1.46 (s, 18H; *t*Bu), 1.54 (s, 9H; *t*Bu), 1.77–1.89 (m, 2H; $OCH_2CH_2C_7H_{14}CH_3$), 4.05 (t, 2H; $^3J_{HH} = 6.6$ Hz, $OCH_2CH_2C_7H_{14}CH_3$), 7.04 (d, 2H, $^3J_{HH} = 8.9$ Hz; c/d-H), 7.65 (d, 2H, $^3J_{HH} = 8.5$ Hz; a/b-H), 7.75 (dd, 2H, $^3J_{HH} = 6.0$ Hz, $^4J_{HH} = 2.1$ Hz; 5-H), 8.02 (d, 2H, $^3J_{HH} = 8.9$ Hz; c/d-H), 8.08 (d, 2H, $^3J_{HH} = 8.5$ Hz; a/b-H), 8.30 (d, 2H, $^4J_{HH} = 2.0$ Hz; 3-H), 8.34 (s, 2H; 3′-H), 9.07 ppm (d with broad ^{195}Pt satellites, 2H, $^3J_{HH} = 6.1$ Hz; 6-H); $^{13}C\{^1H\}$ NMR (126 MHz, CD_3CN, 25 °C, TMS): $\delta = 14.4$, 26.6, 29.8, 30.0, 30.3,30.6, 32.6, 37.1, 38.1, 69.3, 104.0 (PtC≡*C*), 104.2 (Pt*C*≡C), 116.1, 117.2,122.4, 122.8, 124.3, 126.9, 127.5, 129.5, 131.4, 133.4, 155.0, 155.1, 159.8, 163.0, 164.9, 165.4, 168.0, 168.6 ppm; IR (nujol): $\tilde{\nu} = 2118$ cm^{-1} (w, C≡C); MS (FAB, +ve NBA matrix): m/z: 999 $[\mathbf{5}-\text{PF}_6]^+$; elemental analysis: calcd (%) for $C_{53}H_{64}N_5O_2PF_6Pt$: C 55.69, H 5.64, N 6.13; found: C 55.72, H 6.09, N 5.35.

6: 2-(4-Methylphenyl)-5-(4-ethynylphenyl)-[1,3,4]oxadiazole (0.1 mmol) was added to a yellow solution of $[(t\text{Bu}_3\text{tpy})\text{PtCl}]\text{ClO}_4$ (73 mg, 0.10 mmol), CuI (0.01 g, 0.05 mmol), and diisopropylamine (1 mL) in dichloromethane (10 mL). The resultant solution mixture was stirred at room temperature under an inert atmosphere for 12 h. The mixture was evaporated to dryness, dissolved in dichloromethane, and loaded onto an alumina (neutral) column. The orange band was eluted with CH_2Cl_2/MeCN (15:1 v/v), and a yellow band ($R_f = 0.20$) was isolated. $[(t\text{Bu}_3\text{tpy})\text{PtC}\equiv\text{CC}_6\text{H}_4\text{-C}_2\text{N}_2\text{O-C}_6\text{H}_4\text{-CH}_3](\text{ClO}_4)$ (**6**) was obtained as an orange solid (37 mg, 50 %). ^{1}H NMR (500 MHz, CD_3CN, 25 °C): $\delta = 1.47$ (s, 18H; *t*Bu), 1.54 (s, 9H; *t*Bu), 2.41 (s, 3H; CH_3), 7.33 (d, 2H, $^3J_{HH} = 7.9$ Hz; OXD), 7.63 (d, 2H, $^3J_{HH} = 8.5$ Hz; OXD), 7.75 (dd, 2H, $^3J_{HH} = 6.0$ Hz, $^4J_{HH} = 2.1$ Hz; 5-H), 7.96 (d, 2H, $^3J_{HH} = 8.2$ Hz; OXD), 8.08 (d, 2H, $^3J_{HH} = 8.5$ Hz; OXD), 8.30 (d, 2H, $^4J_{HH} = 1.9$ Hz; H$_3$), 8.33 (s, 2H; 3′-H), 9.05 ppm (d with broad ^{195}Pt satellites, 2H, $^3J_{HH} = 6.0$ Hz; 6-H);

$^{13}C\{^1H\}$ NMR (126 MHz, CD_3CN, 25 °C): δ = 21.7, 30.3, 30.6 , 37.1; 38.1, 104.1 (PtC≡*C*), 104.2 (Pt*C*≡C), 122.3, 122.4, 122.7, 124.2, 126.9, 127.5, 127.6, 130.8, 131.5, 133.4, 143.5, 154.9, 155.1, 159.7, 165.2, 165.5, 168.0, 168.6 ppm; IR (nujol): $\tilde{\nu}$ = 2118 cm^{-1} (w, C≡C); MS (FAB, +ve NBA matrix): *m*/*z*: 855 $[\mathbf{6}-ClO_4]^+$; elemental analysis: calcd (%) for $C_{44}H_{46}N_5O_5ClPt\cdot H_2O$: C 54.29, H,4.97, N 7.19; found: C 53.68, H 4.94, N 7.25.

7: The preparation was similar to that for **5** except that 2-(4-dimethylaminophenyl)-5-(4-ethynylphenyl)-[1,3,4]oxadiazole was used instead of 2-(4-methylphenyl)-5-(4-ethynylphenyl)-[1,3,4]oxadiazole. The mixture was stirred for 12 h, evaporated to dryness, dissolved in dichloromethane, and loaded onto an alumina (neutral) column. The orange band was eluted with CH_2Cl_2 (R_f = 0.20), and upon evaporation gave [(*t*Bu_3tpy)PtC≡CC_6H_4-C_2N_2O-C_6H_4-$N(CH_3)_2$](PF_6) as an orange solid (88 mg, 86 %). ^1H NMR (500 MHz, CD_3CN/$[D_6]$DMSO (1:1 *v*/*v*), 25 °C, TMS): δ = 1.46 (s, 18H; *t*Bu), 1.55 (s, 9H; *t*Bu), 3.04 (s, 6H; $N(CH_3)_2$), 6.84 (d, 2H, $^3J_{HH}$ = 9.0 Hz; OXD), 7.67 (d, 2H, $^3J_{HH}$ = 8.4 Hz; OXD), 7.85 (dd, 2H, $^3J_{HH}$ = 6.0 Hz, $^4J_{HH}$ = 2.1 Hz; 5-H), 7.92 (d, 2H, $^3J_{HH}$ = 9.0 Hz; OXD), 8.06 (d, 2H, $^3J_{HH}$ = 8.3 Hz; OXD), 8.64 (d, 2H, $^4J_{HH}$ = 2.0 Hz; 3-H), 8.66 (s, 2H; 3′-H), 9.06 ppm (d, 2H, $^3J_{HH}$ = 6.0 Hz; 6-H); $^{13}C\{^1H\}$ NMR (126 MHz, CD_3CN/$[D_6]$DMSO (1/1 *v*/*v*), 25 °C, TMS): δ = 29.9, 30.4, 36.5, 37.5, 103.5 (PtC≡*C*), 104.2 (Pt*C*≡C), 110.4, 112.1, 119.0, 121.9, 123.9, 126.2, 126.6, 128.3, 130.4, 132.7, 152.8, 154.1, 154.2, 159.0, 163.2, 165.1, 167.0, 167.7 ppm; IR (nujol): $\tilde{\nu}$ = 2116 cm^{-1} (w, C≡C); MS (FAB, +ve NBA matrix): *m*/*z*: 883 $[\mathbf{7}-PF_6]^+$; elemental analysis: calcd (%) for $C_{45}H_{49}N_6OPtPF_6\cdot 2H_2O$: C 50.70, H 5.01, N 7.88; found: C 50.53, H 4.65, N 7.64.

8: 2-(4-Methylphenyl)-5-(4-ethynylphenyl)-[1,3,4]oxadiazole (0.12 mmol) was added to a yellow solution of [(C^N^N)PtCl] (57 mg, 0.12 mmol), CuI (0.01 g, 0.05 mmol), and diisopropylamine (1 mL) in dichloromethane (15 mL). The resultant solution mixture was stirred at room temperature under inert atmosphere for 12 h. The mixture was evaporated to dryness, dissolved in dichloromethane, and loaded onto an alumina (neutral) column. The orange band was eluted with CH_2Cl_2/*n*-hexane (5:1 *v*/*v*) (R_f = 0.36). Orange needles of [(C^N^N)PtC≡CC_6H_4-C_2N_2O-C_6H_4-CH_3](PF_6) (49 mg, 60 %) were obtained by slow diffusion of diethyl ether into a solution in dichloromethane. ^1H NMR (500 MHz, $[D_6]$DMSO, 25 °C, TMS): δ = 2.42 (s, 3H; CH_3), 7.08 (t, 1H, $^3J_{HH}$ = 7.4 Hz; C^N^N), 7.14 (t, 1H, $^3J_{HH}$ = 7.3 Hz; C^N^N), 7.44 (d, 2H, $^3J_{HH}$ = 8.0 Hz; OXD), 7.59 (d, 2H, $^3J_{HH}$ = 8.5 Hz; OXD), 7.65–7.67 (m, 1H; C^N^N), 7.75–7.77 (m, 1H; C^N^N), 7.87–7.90 (m, 1H; C^N^N), 8.03 (d, 5H, $^3J_{HH}$ = 8.4 Hz; OXD and C^N^N), 8.15 (t, 1H, $^3J_{HH}$ = 8.0 Hz; C^N^N), 8.24–8.26 (m, 1H; C^N^N), 8.36 (t, 1H, $^3J_{HH}$ = 7.8 Hz; C^N^N), 8.52–8.54 (m, 1H; C^N^N), 9.06 ppm (d, 1H, $^3J_{HH}$ = 4.4 Hz, C^N^N); ^{13}C NMR (126 MHz, $[D_6]$DMSO, 25 °C, TMS): δ = 21.2, 105.2 (PtC≡*C*), 110.4 (Pt*C*≡C), 114.9, 118.1, 119.3, 119.4, 120.7, 123.8, 124.2, 125.1, 126.5, 126.6, 128.8, 130.0, 130.8, 131.9; 132.5, 140.3, 140.4, 142.1, 147.2, 154.4, 157.5, 163.8, 163.9, 164.1 ppm; IR (nujol): $\tilde{\nu}$ = 2089 cm^{-1} (m, C≡C); MS (FAB, +ve NBA matrix): *m*/*z*: 687 $[\mathbf{8}+H]^+$; elemental analysis: calcd (%) for $C_{33}H_{22}N_4OPt\cdot H_2O$: C 56.33, H 3.44, N 7.96; found: C 56.26, H 3.38, N 7.65.

X-ray Crystallography

Crystals of **5**·2MeCN and **8** were obtained by slow diffusion of diethyl ether into a solution of **5** in acetonitrile and a solution of **8** in dichloromethane, respectively. A yellow crystal of **5**·2MeCN of dimensions 0.6 mm × 0.25 mm × 0.15 mm with mother liquor and an orange crystal of **8** of dimensions of 0.5 mm × 0.25 mm × 0.15 mm were mounted on glass capillaries for data collection at −20 °C on a MAR diffractometer with a 300-mm image plate detector by using graphite monochromated $Mo_{K\alpha}$ radiation (λ = 0.71073 Å). The images were interpreted and intensities integrated by using the program DENZO.[30] The structures were solved by direct methods employing the SIR-97 program[31] on PC. Pt, and many non-hydrogen atoms were located according to direct methods and successive least-square Fourier cycles. The positions of other non-hydrogen atoms were found after successful refinement by full-matrix least-squares by using the program SHELXL-97[32] on PC. The positions of hydrogen atoms were calculated based on the riding mode with thermal parameters equal to 1.2 times that of the associated C atoms, and included in the calculation of final *R* indices. For **5**·2MeCN, one crystallographic asymmetric unit consists of one formula unit, including two anions and two acetonitrile molecules, whereas for **8**, there was one crystallographic asymmetric unit consisting of one formula unit. In the final stage of least-squares refinement, non-hydrogen atoms of acetonitrile and F atoms were refined isotropically and other non-hydrogen atoms were refined anisotropically for **5**·2MeCN, whereas in the case of **8**, all non-hydrogen atoms were refined anisotropically. Hydrogen atoms of **5**·2MeCN (except those on the acetonitrile molecules) and all non-hydrogen atoms of **8** were generated by the program SHELXL-97.[32] See Supporting Information for crystal data, details of collection, and refinement. CCDC 609768 and 609769 contain the supplementary crystallographic data for this paper. These data can be obtained free of charge from The Cambridge Crystallographic Data Centre via www.ccdc.cam.ac.uk/data_request/cif.

Acknowledgements

This work was supported by the Area of Excellence Scheme established under the University Grants Committee of the Hong Kong SAR, China (AoE/P-10/01) and the Strategic Research Themes on "Bio-nanotechnology", "Organic Optoelectronics" and "Nanotechnology Research Program" of the University Development Fund of The University of Hong Kong. W.L. thanks The University of Hong Kong for a University Postdoctoral Fellowship and the Small Project Funding. We thank Mr. Lee Wing Sang in the Electron Microscope Unit of the University of Hong Kong for technical assistance and Dr. Rory M. Watt for his help in editing this manuscript.

[1] a) P. Terech, R. G. Weiss, *Chem. Rev.* **1997**, *97*, 3133–3159; b) J. H. van Esch, B. L. Feringa, *Angew. Chem.* **2000**, *112*, 2351–2354; *Angew. Chem. Int. Ed.* **2000**, *39*, 2263–2266; c) N. M. Sangeetha, U. Maitra, *Chem. Soc. Rev.* **2005**, *34*, 821–836; d) M. de Loos, B. L. Feringa, J. H. van Esch, *Eur. J. Org. Chem.* **2005**, 3615–3631; e) J. H. Jung, S. Shinkai, *Top. Curr. Chem.* **2005**, *248*, 223–260; f) *Molecular Gels—Materials with Self-Assembled Fibrillar Networks* (Eds.: R. G. Weiss, P. Terech), Springer, Dordrecht, **2005**.

[2] a) P. C. Griffiths, M. Côte, R. James, P. G. Rogueda, I. R. Morgan, D. W. Knight, *Chem. Commun.* **2005**, 3998–4000; b) A. Ikeda, K. Sonoda, M. Ayabe, S. Tamaru, T. Nakashima, N. Kimizuka, S. Shinkai, *Chem. Lett.* **2001**, 1154–1155; c) N. Mohmeyer, P. Wang, H.-W. Schmidt, S. M. Zakeeruddin, M, Grätzel, *J. Mater. Chem.* **2004**, *14*, 1905–1909.

[3] To our knowledge, there are only three organogelators in the literature bearing no steroidal moieties, hydrogen-bonding motifs, and long alkyl side chains: a) B. K. An, D. S. Lee, J. S. Lee, Y. S. Park, H. S. Song, S. Y. Park, *J. Am. Chem. Soc.* **2004**, *126*, 10232–10233; b) T. Ishi-I, T. Hirayama, K. Murakami, H. Tashiro, T. Thiemann, K. Kubo, A. Mori, S. Yamasaki, T. Akao, A. Tsuboyama, T. Mukaide, K. Ueno, S. Mataka, *Langmuir* **2005**, *21*, 1261–1268; c) S. J. Langford, M. J. Latter, V. L. Lau, L. L. Martin, A. Mechler, *Org. Lett.* **2006**, *8*, 1371–1373.

[4] P. Terech, C. Chachaty, J. Gaillard, A. M. Godquin-Giroud, *J. Phys. F* **1987**, *48*, 663–671.

[5] G. Bühler, M. C. Feiters, R. J. M. Nolte, K. H. Dötz, *Angew. Chem.* **2003**, *115*, 2599–2602; *Angew. Chem. Int. Ed.* **2003**, *42*, 2494–2497.

[6] a) M. Shirakawa, N. Fujita, T. Tani, K. Kanebo, S. Shinkai, *Chem. Commun.* **2005**, 4149–4151; b) M. Shirakawa, N. Fujita, T. Tani, K. Kanebo, M. Ojima, A. Fujii, M. Ozaki, S. Shinkai, *Chem. Eur. J.* **2007**, *13*, 4155–4162.

[7] S.-j. Kawano, N Fujita, S. Shinkai, *J. Am. Chem. Soc.* **2004**, *126*, 8592–8593.

[8] K. Kuroiwa, T. Shibata, A. Takada, N. Nemoto, N. Kimizuka, *J. Am. Chem. Soc.* **2004**, *126*, 2016–2021.

[9] A. Kishimura, T. Yamashita, T. Aida, *J. Am. Chem. Soc.* **2005**, *127*, 179–183.
[10] a) S. Tamaru, M. Nakamura, M. Takeuchi, S. Shinkai, *Org. Lett.* **2001**, *3*, 3631–3634; b) S. Tamaru, S. Uchino, M. Takeuchi, M. Ikeda, T. Hatano, S. Shinkai, *Tetrahedron Lett.* **2002**, *43*, 3751–3755.
[11] T. Klawonn, A. Gansäuer, I. Winkler, T. Lauterbach, D. Franke, R. J. M. Nolte, M. C. Feiters, H. Börner, J. Hentschel, K. H. Dötz, *Chem. Commun.* **2007**, 1894–1895.
[12] a) F. Camerel, R. Ziessel, B. Donnio, C. Bourgogne, D. Guillon, M. Schmutz, C. Iacovita, J. P. Bucher, *Angew. Chem.* **2007**, *119*, 2713–2716; *Angew. Chem. Int. Ed.* **2007**, *46*, 2659–2662; b) A. Y. Y. Tam, K. M. C. Wong, G. X. Wang, V. W. W. Yam, *Chem. Commun.* **2007**, 2028–2030.
[13] T. Tu, W. Assenmacher, H. Peterlik, R. Weisbarth, M. Nieger, K. H. Dötz, *Angew. Chem.* **2007**, *119*, 6486; *Angew. Chem. Int. Ed.* **2007**, *46*, 6368-6371.
[14] F. Fages, *Angew. Chem.* **2006**, *118*, 1710–1712; *Angew. Chem. Int. Ed.* **2006**, *45*, 1680–1682.
[15] a) T. Naota, H. Koori, *J. Am. Chem. Soc.* **2005**, *127*, 9324–9325; b) K. Isozaki, H. Takaya, T. Naota, *Angew. Chem.* **2007**, *119*, 2913–2915; *Angew. Chem. Int. Ed.* **2007**, *46*, 2855–2857.
[16] a) K. W. Jennette, S. J. Lippard, G. A. Vassiliades, W. R. Bauer, *Proc. Natl. Acad. Sci. USA* **1974**, *71*, 3839–3843; b) A. H. J. Wang, J. Nathans, G. Van der Marel, J. H. Van Boom, A. Rich, *Nature* **1978**, *276*, 471–474; c) H. M. Brothers II, N. M. Kostic, *Inorg. Chem.* **1988**, *27*, 1761–1767; d) C. S. Peyratout, T. K. Aldridge, D. K. Crites, D. R. McMillin, *Inorg. Chem.* **1995**, *34*, 4484–4489; e) J. A. Bailey, M. G. Hill, R. E. March, V. M. Miskowski, W. P. Schaefer, H. B. Gray, *Inorg. Chem.* **1995**, *34*, 4591–4599.
[17] a) V. W. W. Yam, R. P. L. Tang, K. M. C. Wong, K. K. Cheung, *Organometallics* **2001**, *20*, 4476–4482; b) Q. Z. Yang, L. Z. Wu, Z. X. Wu, L. P. Zhang, C. H. Tung, *Inorg. Chem.* **2002**, *41*, 5653–5655; c) W. Lu, B. X. Mi, M. C. W. Chan, Z. Hui, N. Y. Zhu, S. T. Lee, C. M. Che, *Chem. Commun.* **2002**, 206–207; d) V. W. W. Yam, K. M. C. Wong, N. Y. Zhu, *Angew. Chem.* **2003**, *115*, 1438–1441; *Angew. Chem. Int. Ed.* **2003**, *42*, 1400–1403.
[18] a) S. Y. Ryu, S. Kim, J. Seo, Y. W. Kim, O. H. Kwon, D. J. Jang, S. Y. Park, *Chem. Commun.* **2004**, 70–71; b) G. Hughes, D. Kreher, C. S. Wang, A. S. Batsanov, M. R. Bryce, *Org. Biomol. Chem.* **2004**, *2*, 3363–3367; c) C. Wang, L. O. Pålsson, A. S. Batsanov, M. R. Bryce, *J. Am. Chem. Soc.* **2006**, *128*, 3789–3799.
[19] G. Hughes, M. R. Bryce, *J. Mater. Chem.* **2005**, *15*, 94–107.
[20] S. W. Lai, M. C. W. Chan, K. K. Cheung, C. M. Che, *Inorg. Chem.* **1999**, *38*, 4262–4267.
[21] a) C. A. Hunter, J. K. M. Sanders, *J. Am. Chem. Soc.* **1990**, *112*, 5525–5534; b) W. Lu, M. C. W. Chan, K. K. Cheung, C. M. Che, *Organometallics* **2001**, *20*, 2477–2486; c) W. Lu, M. C. W. Chan, N. Y. Zhu, C. M. Che, C. Li, Z. Hui, *J. Am. Chem. Soc.* **2004**, *126*, 7639–7651.
[22] *Textures of Liquid Crystals* (Ed.: I. Dierking), Wiley-VCH, Weinheim, **2003**.
[23] B. Mohr, G. Wegner, K. Ohta, *J. Chem. Soc. Chem. Commun.* **1995**, 995–996.
[24] a) S. Kumer, E. J. Wachtel, E. Keinan, *J. Org. Chem.* **1993**, *58*, 3821–3827; b) T. Sauer, *Macromolecules* **1993**, *26*, 2057–2063.
[25] T. Kitahara, M. Shirakawa, S.-i. Kawano, U. Beginn, N. Fujita, S. Shinkai, *J. Am. Chem. Soc.* **2005**, *127*, 14980–14981.
[26] A. J. Lovinger, C. Nuckolls, T. J. Katz, *J. Am. Chem. Soc.* **1998**, *120*, 264–268.
[27] S. X. Xiao, J. Y. Yang, T. Beetz, X. F. Guo, N. Tremblay, T. Siegrist, Y. M. Zhu, M. Steigerwald, C. Nuckolls, *J. Am. Chem. Soc.* **2006**, *128*, 10700–10701, and references therein.
[28] T. Yamamoto, D. Komarudin, M. Arai, B. L. Lee, H. Suganuma, N. Asakawa, Y. Inoue, K. Kubota, S. Sasaki, T. Fukuda, H. Matsuda, *J. Am. Chem. Soc.* **1998**, *120*, 2047–2058.
[29] a) D. J. Abdallah, R. G. Weiss, *Langmuir* **2000**, *16*, 352–355; b) D. J. Abdallah, S. A. Sirchio, R. G. Weiss, *Langmuir* **2000**, *16*, 7558–7561.
[30] Z. Otwinowski, W. Minor, *Methods Enzymol.* **1997**, *276*, 307–326.
[31] A. Altomare, M. C. Burla, M. Camalli, G. Cascarano, C. Giacovazzo, A. Guagliardi, A. G. G. Moliterni, G. Polidori, R. Spagna, *J. Appl. Crystallogr.* **1999**, *32*, 115–119.
[32] G. M. Sheldrick, SHELXL97, Programs for Crystal Structure Analysis (Release 97-2), University of Goetingen, Germany, **1997**.

Received: August 24, 2007
Published online: December 4, 2007

